Batteries & Supercaps

Research Article
doi.org/10.1002/batt.202400741

Chemistry Europe
European Chemical Societies Publishing

www.batteries-supercaps.org

Engineering Current Collector with 2D TiO_2 Nanosheets for Stable Lithium Metal Batteries

Jun Seo Park,[a] Mohammad Nasir,[a, b] Donghyoung Kim,[c] Hyung Mo Jeong,*[c] and Hee Jung Park*[a, b]

The formation of lithium dendrites, driven by the non-uniform deposition of lithium, remains a critical challenge for the performance and safety of lithium metal batteries. To address this issue, we engineer the surface of copper current collectors by depositing ultra-thin 2D TiO2 nanosheets with varying thicknesses (0–1200 nm) as a protective layer. Half-cells without the 2D TiO2 coating exhibit a significant decline in Coulombic efficiency after only 65 charge-discharge cycles. In contrast, the modified current collector with the smoothest surface achieves remarkable cycling stability, maintaining ~97.6% Coulombic efficiency after 200 cycles. Full cells incorporating these nanosheets demonstrate a good discharge capacity of ~134 mAh/g after 150 cycles at a 1 C rate. The improved electrochemical performance is attributed to the high lithium affinity and reduced surface roughness of the current collector facilitated by the 2D TiO_2 buffer layer. These findings emphasize the crucial role of 2D TiO_2 nanosheets in regulating Li-ion deposition, thereby significantly improving the cycling stability and performance of lithium metal batteries.

Introduction

Over the last decade, the demand for high-energy-density batteries, driven by the electric vehicle and consumer electronics industries, has significantly increased. The energy density of lithium-ion batteries (LIBs) based on liquid electrolytes utilizing graphite as an anode has already reached its theoretical limit.[1] With its high theoretical capacity and suitable operating voltage, silicon (Si) is the next cathode material of choice for LIBs. However, silicon anodes have problems such as severe volume expansion and low electronic conductivity.[2] In comparison, lithium-metal batteries (LMBs) achieve high energy density due to the utilization of lithium metal with a high specific capacity (3860 mAh/g) and low redox potential (−3.040 V vs. standard hydrogen electrode) as an anode.[3–5] Furthermore, the use of lithium metal anodes facilitates the development of lithium-air cells with high energy density.[6] However, Li dendrites tend to form during repeated deposition and stripping of lithium metal due to non-uniform lithium deposition in LMBs. Dendritic growth can not only lead to internal short circuits or thermal runaway but also reduce the reversibility of lithium generation reactions due to side reactions between lithium and the liquid electrolyte.[7–9] Consequently, the structural and chemical instability of lithium severely affects battery performance.[10,11]

Several approaches have been proposed to address the issues concerning dendrite growth in LMBs. These include the utilization of solid electrolyte,[12–14] modifying the liquid electrolyte,[15,16] introducing an artificial solid-electrolyte interphase (SEI) layer,[17] and modifying the separator[18] and the current collector.[19–31] In particular, modifications to the current collector can contribute to the development of anode-less cells, which enhance battery energy density by eliminating the need for lithium metal.[32,33] For example, additives such as $LiNO_3$, LiF, and vinylene carbonate have been incorporated into the electrolyte to form a stable SEI layer with Li metal, as the common liquid electrolyte can lead to an unstable SEI layer, accelerating dendrite growth.[15,16] Li et al. introduced Li_3PO_4 having high Young modulus as artificial SEI layer which have effectively suppressed side reactions between Li metal and electrolyte.[17] Lee et al. modified the separator by Cu coating to inhibit dendritic growth and improve cycle stability.[18] The ultra-thin Cu film plays a dual role, by discouraging accumulation of dead Li and enhancing ionic conduction. As a result, morphological uniformity of Li deposition and thermal stability of separator was improved.

Additionally, alternative strategies such as introducing lithophilic interlayers (electrode modification) have been explored. Hou et al. demonstrated that nanostructured lithiophilic Ag layer coated on Cu substrate (by electrodeless plating) reduces the nucleation overpotential by inducing uniform Li flux.[22] Similarly, C. Zhang et al. grew vertically aligned CuO nanofilm on Cu substrates.[21] The CuO film layer acts as a lithiophilic layer and thus promotes the rapid transport of Li

[a] J. S. Park, M. Nasir, H. J. Park
Department of Materials Science and Engineering
Dankook University
Dandae-ro 119, Cheonan 31116, Korea
E-mail: parkjang@dankook.ac.kr

[b] M. Nasir, H. J. Park
Hydrogen Research Center
Dankook University
Dandae-ro 119, Cheonan 31116, Korea

[c] D. Kim, H. M. Jeong
School of Mechanical Engineering and Department of Smart Fab. Technology
Sungkyunkwan University
Seobu-ro 2066, Suwon 16419, Korea
E-mail: hmjeong@skku.edu

Supporting information for this article is available on the WWW under https://doi.org/10.1002/batt.202400741

Research Article
doi.org/10.1002/batt.202400741
Chemistry Europe
European Chemical Societies Publishing

ions, resulting in stable nucleation and stable cycling characteristics. Moreover, 2D materials such carbon nanotubes (CNTs) with exposed basal plane have also been used as protective layer as they can store sufficient Li ions and facilitate more uniform Li flux.[25]

Although the aforementioned methods improve lithiophilicity, lithium dendrite growth still persists under high current densities and prolonged cycling. Therefore, it seems that an ideally smooth (atomically flat) Cu current collector with Li-affinity sites could effectively resolve dendrite growth issues in LMBs. However, achieving an atomically uniform surface in constituent materials (current collector, SEI layer, separator, lithium metal), which have a three-dimensional (3D) structure, is challenging due to their inherent structural limitations (such as dangling bonds, leading to inevitable surface roughness).[34] To this end, we propose the use of 2D metal oxide nanosheets with their fully exposed basal planes as a protective layer to effectively regulation Li flux for inhibit dendrite growth. In this study, the 2D titanium oxides nanosheets with varying thicknesses were coated onto the Cu current collector. Consequently, charge-discharge cycling of LMBs with modified current collector was investigated. The half-cell exhibited excellent cycling stability of ~97.6% after 200 cycles due to the controlled Li growth facilitated by the 2D TiO_2 layer.

Results and Discussion

To prepare 2D TiO_2 nanosheets, the layered mother phase (KTLO) was first prepared using flux crystal growth technique. The digital image of synthesized KTLO crystals is shown in Figure 1a and the zoomed view is depicted in Figure 1b. The acidic treatment of KTLO was performed in 1 M HCl to interchange K^+ by hydronium ions to form hydrated TiO_2 ($TiO_2 \cdot nH_2O$, HTO) (Figure 1c). Organic treatment, followed by dialysis process, was carried out using tetrabutylammonium hydroxide (TBAOH) to facilitate TiO_2 exfoliation into nanosheet colloids (Figure 1d). The morphology of 2D TiO_2 nanosheets was investigated using STEM, SAED, and AFM. As shown in Figure 1e–f image shows the successful exfoliation of layered structure into the nanosheets, with a thickness of a few nm and in-plane size of micrometers. In addition, the peak of the stack structure of 2D TiO_2 is observed in the XRD analysis results of Figure S1. The nanosheets were found crystalline in nature as observed from selective area electron diffraction (SAED) analysis (inset; Figure 1e). As shown in Figure 1g, HRTEM also exhibits a planar crystal structure of 2D TiO_2 nanosheets. STEM-EDX analysis was performed to investigate the chemical composition of 2D TiO_2 nanosheets. The EDX analysis results in Figure 1h show that Ti and O atoms are distributed very evenly in 2D TiO_2 nanosheets. And it turns out that the O/Ti ratio is ~3.6. The oxygen excess (Ti deficiency) state of 2D TiO_2 nanosheets results from the structure of KTLO and creates a negatively charged surface (−81.5 mV. See Figure S2). The nanosheets with varying thicknesses were uniformly coated on Cu substrate by electrophoresis technique by applying different voltage ranging from 2 V to 8 V.

Figure 2a shows the photographs of 2D TiO_2-coated copper substrates along with bare copper current collector. Depending on the voltage applied during electrophoresis procedure, the TiO_2 film thickness on Cu was measured to be 0 nm (no-coating, NS-0), ~250 nm (NS-250), ~450 nm (NS-450), ~600 nm (NS-600), and ~1200 nm (NS-1200), as illustrated in Figure 2b–e. 2D TiO_2 coated film shows good adhesiveness and flexibility without any obvious cracks upon bending as illustrated in Figure S3. Figure 2(f and g) shows the representative AFM images of NS-0 and NS-600 samples. The average root mean square (rms) surface roughness values were ~59 nm for NS-0, ~44 nm for NS-250, ~33 nm for NS-450, ~34 nm for NS-600, and ~44 nm for NS-1200, as determined from AFM studies. This indicates that the surface roughness is strongly influenced by TiO_2 nanosheet

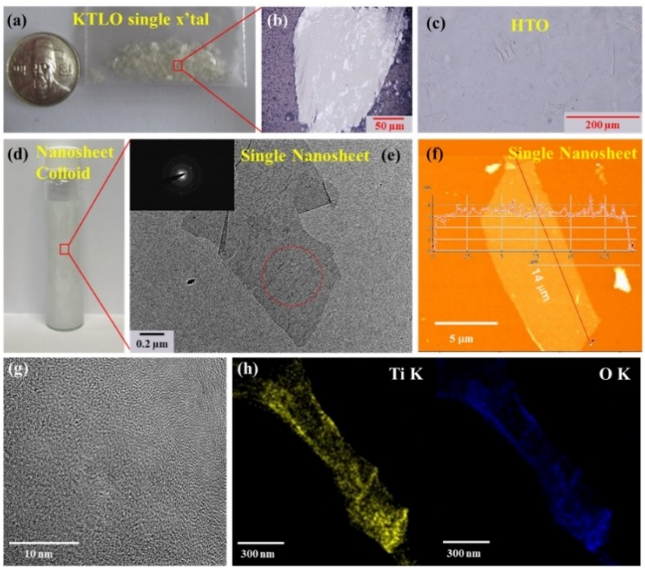

Figure 1. Characterization of 2D TiO_2 nanosheet: (a) digital photo of the single crystal KTLO, optical microscope images of (b) KTLO and (c) HTO. (d) 2D TiO_2 nanosheet colloid and (e) TEM (including SAED pattern) (f) AFM images of 2D TiO_2 nanosheet. (g) HR-TEM images of 2D TiO_2 nanosheets. (h) EDX mapping images of 2D TiO_2 nanosheets.

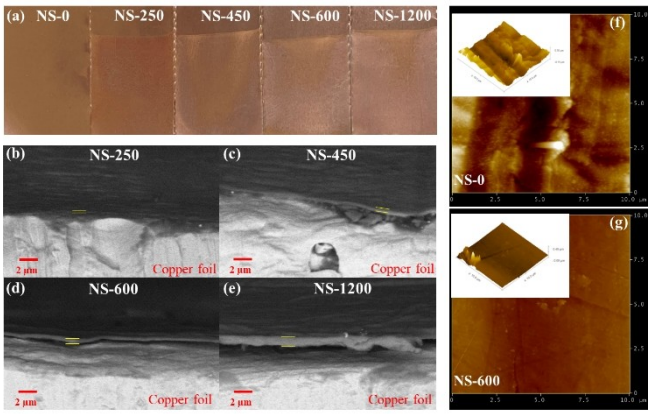

Figure 2. Characterization of 2D TiO_2 nanosheet coated on copper substrate: (a) digital images of the copper substrate coated with 2D TiO_2 nanosheets (NS-0~NS-1200), (b–e) SEM images of NS-#, and AFM images of (f) NS-0 and (g) NS-600.

Research Article
doi.org/10.1002/batt.202400741
Chemistry Europe
European Chemical Societies Publishing

deposition on Cu. The NS-0 sample without TiO_2 coating exhibits largest surface roughness, while NS-450 samples reveal a highly smooth surface with lowest surface roughness among all samples. The electrochemical performance of TiO_2 nanosheets was examined under a half cell (2032-coin cell) configuration. The samples, NS-0, NS-250, NS-450, NS-600, and NS-1200 were employed as the working electrodes, while Li metal foil was used as the counter electrode. A schematic of an assembled half-cell based on TiO_2 nanosheets is shown in Figure 3a. The cycle performance of the cells was assessed by recording charge-discharge curves at a current density of 1 mA/cm^2 and an areal capacity of 1 mAh/cm^2 at 25 °C. The charge-discharge curves are depicted in Figure 3b,d. The charge-discharge curves for the 1st and 50th cycles are shown in Figure 3c,d respectively. The observed charge-discharge characteristics closely match with the typical cycling features reported for conventional LMBs (Figure 3b. Note that total overpotential (V_t) consists of nucleation overpotential (V_n) and polarization overpotential (V_p)).[35] Initially, during charging, cell potential drops sharply to a minimum value and then increases and becomes saturate to V_p for all samples (eventually, $V_t \approx V_p$ after a certain time) (Figure 3c). was observed for the uncoated sample as compared to coated samples. However, the 2D TiO_2 coated samples reveal lesser V_p, compared to the uncoated sample during charging-discharging (inset II, Figure 3c) (Red

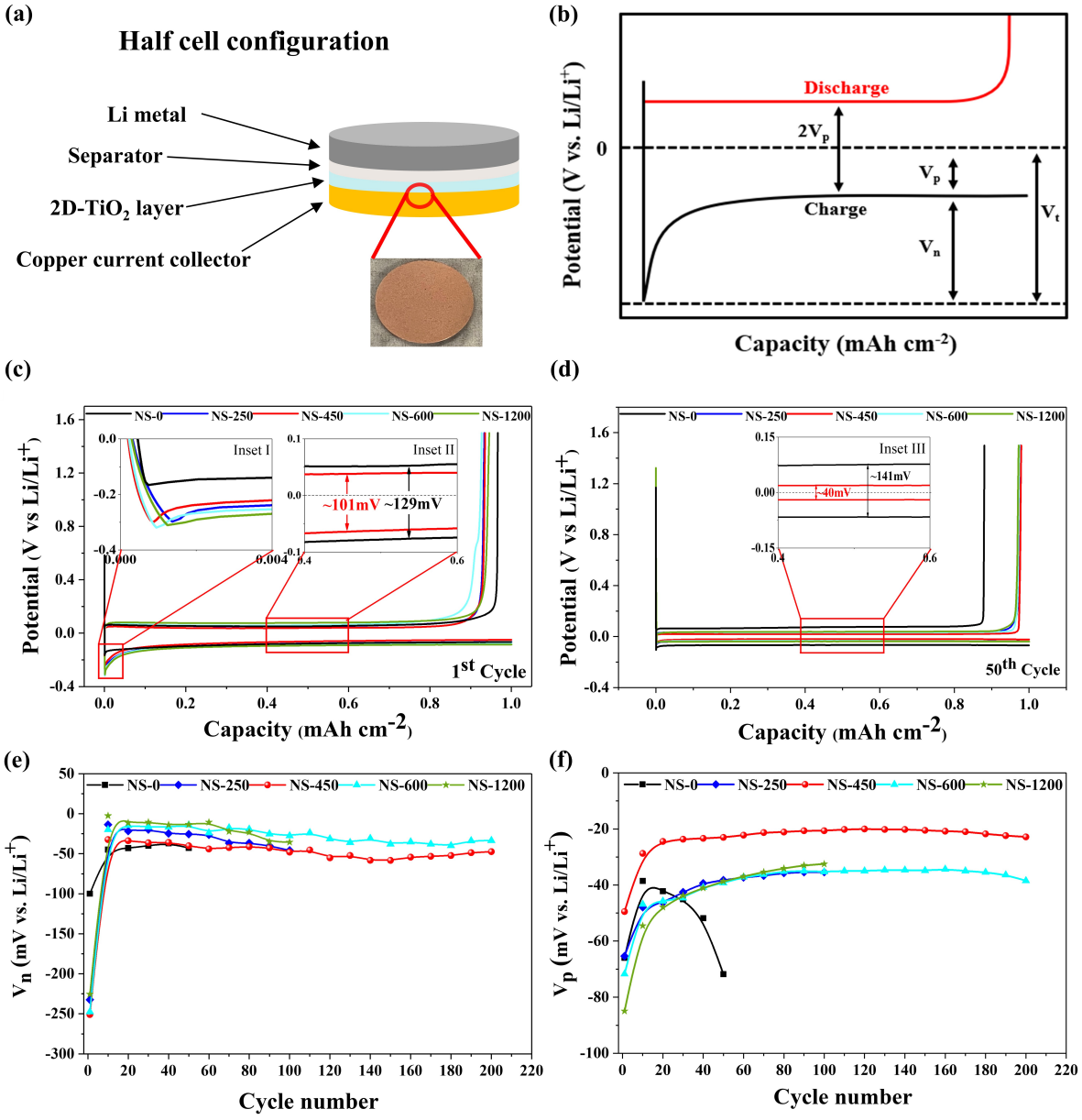

Figure 3. (a) Schematic of NS-# half-cell configuration: charge-discharge curves of (b) conventional LMBs, (c) NS-# half-cells in the first cycle, and (d) NS-# half-cell at the 50th cycle. (e) nucleation overpotential (V_n) and (f) polarization overpotential (V_p) of NS-# half-cells for selected number of cycles. V_t denotes total overpotential, i.e., $V_t \sim V_p + V_n$.

Research Article
doi.org/10.1002/batt.202400741
Chemistry Europe
European Chemical Societies Publishing

and black lines indicate with/without coating samples, respectively).

For instance, the polarization overpotential of NS-450 was ~101 mV ($2V_p$), while that of NS-0 was ~129 mV ($2V_p$). After 50th cycle, the difference in V_p becomes more pronounced for 2D TiO_2 coated and uncoated nanosheets (Figure 3d). The polarization overpotential of NS-450 and NS-0 were ~40 mV and ~141 mV, respectively (inset; Figure 3d). The V_n and V_p (as a function of cycle numbers) are summarized in Figure 3e and f, respectively, for all samples. A similar trend of V_n is observed for all coated samples. However, coated samples exhibit higher values of V_n for the first cycle. This may be attributed to higher resistance (ohmic resistance) for lithium nucleation offered by the titanium-oxide layer. However, as the cycling progresses, V_n for coated samples become smaller than that without coating. Once nucleation has been achieved, V_n is generally reduced by the residual lithium layer even after repeated cycling (homogeneous nucleation), regardless of the presence or absence of the coating layer.[35,36] Importantly, V_p, a crucial parameter for cycling stability, decreases during cycling for 2D TiO_2 coated samples (NS-#), whereas the value increases for NS-0 (Figure 3f). This may be attributed to the smooth and lithiophilic surface formation by the 2D TiO_2 layer (Note that the surface of 2D TiO_2 has negative charge). The reduction in V_p leads to high Coulombic efficiency, which can be computed from the change of the capacity as per cycling. From Figure 3c and d, it can be observed that the discharge curve for NS-0 shifts to the left side of the *x*-axis, whereas NS-# nearly remains unchanged after the 50th cycle. This indicates that 2D TiO_2 layer maintains the capacities well for NS-# as compared to one without coating (NS-0). Hence, relatively higher Coulombic efficiency (charge capacity/discharge capacity ×100%) for the charge-discharge cycle in NS-# is expected.

From Figure 4a, it is observed the Coulombic efficiency for NS-0 was measured to be ~80% after 66 cycles. On the other hand, 2D TiO_2 layer coated samples exhibit significantly higher coulombic efficiencies. The Coulombic efficiency is found to vary with the samples thickness. It is worth noting that NS-450 samples show highest Coulombic efficiency ~98% after 50 cycles and the efficiency is almost maintained up to 200 cycles. In addition, the high coulombic efficiency (~95%) is maintained at higher current density of 2 mA/cm^2 and 3 mA/cm^2 upto 150 cycle (Figure S4). This improvement for NS-#s in cycling characteristics may be associated with the chemical and physical changes in Cu current collector due the 2D TiO_2 coating layer. The 2D TiO_2 coating layer provides Li-affinitive Ti-sites for Li stripping and plating. This effect has similar impact (it can be assumed that 2D layers have similar Li-affinity Li ion, *i.e.*, similar chemical factor) for all coated samples, irrespective of sample thickness. However, no reasonable relationship was observed in cycling performance with the TiO_2 film thickness, as shown in Figure 4b. Interestingly, a systematic trend in cycling characteristics of cell is observed with surface roughness as shown in Figure 4c. This implies that cycling performance is strongly influenced by the physical factor, *i.e.*, surface roughness. The cycling performance decreases with increasing surface roughness. The NS-450 with relatively smaller roughness, shows highest cycling performance. It appears that surface roughness correlates with the surface reaction, *i.e.*, the polarization resistance (V_p), while the film thickness may be linked to the

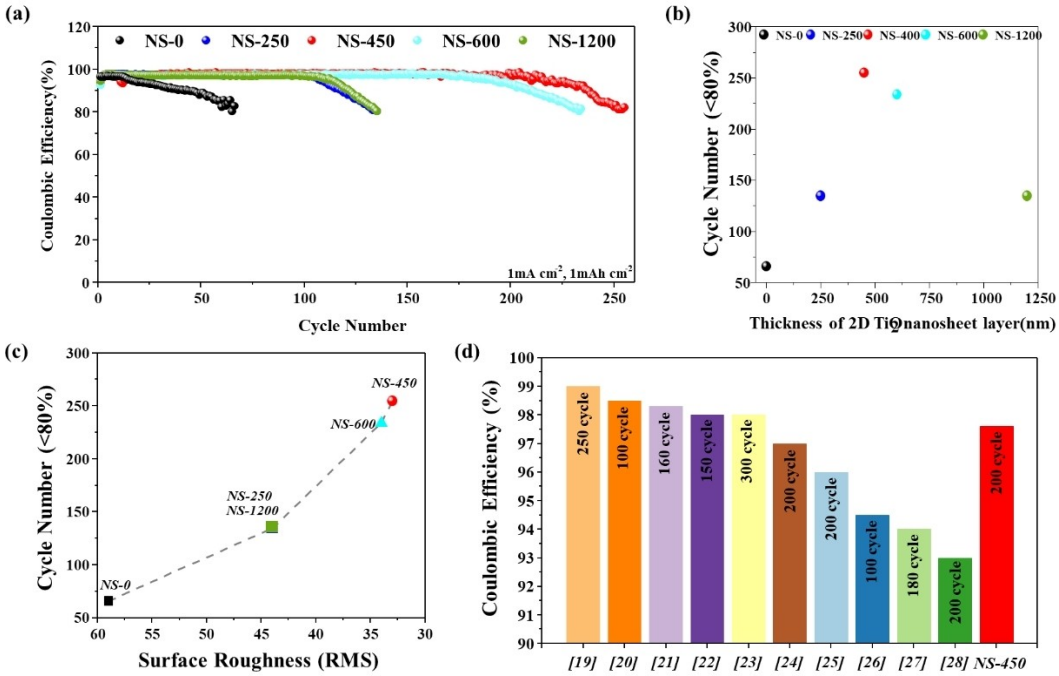

Figure 4. NS-# half-cell electrochemical properties: (a) Coulombic efficiency of NS-# half-cell as a function of cycling. (b) Variation of cycle number with thickness of 2D TiO_2 film coated on the copper substrate. (c) number of cycling *vs.* the surface roughness plot of the copper substrate with/without 2D TiO_2 film. (d) comparison of cycle number and coulombic efficiency between the previously reported samples and NS-450 (this study). Red bar is the result of NS-450.

Research Article
doi.org/10.1002/batt.202400741
Chemistry Europe
European Chemical Societies Publishing

ohmic resistance of the cell. Therefore, smaller V_p in NS-450 associated with low surface roughness seems advantageous for enhancing cycling characteristics. This underscores the role of TiO_2 nanosheets in reducing surface roughness (thus reducing V_p) providing a homogeneous and lithophilic surface on Cu, which hinders the dendrite growthLastly, in Figure 4d, the cycling characteristics (cycling number and coulombic efficiency) of NS-450 are compared with the previous reports on Li Li-metal batteries where different strategies have been applied to prevent Li-dendrite. Although the cell structure may vary, the data is compared under same experimental conditions (current density ~1 mA/cm^2, specific capacity ~1 mAh/cm^2). Except few studies (~300 cycles and Coulombic efficiency ~98 %), the NS-450 sample studied here shows better cycling characteristic compared to previously reported strategies. (17–26) Conclusively, this result demonstrates that the incorporation of a 2D coating film with lithiophilic surface and low surface roughness between the copper current collector and the liquid electrolyte effectively suppresses dendrite growth in LMBs and, even in anode-free batteries, thereby further enhancing cell cycling performance.

To get insight into improved electrochemical performance of 2D TiO_2 coated sample, the impedance patterns of NS- 0 and NS-450 half cells have been compared after the 1st and 50th cycles (Figure 5a,b). It has been observed that the NS-450 half-cell shows lower resistance compared to NS-0 half-cell. Also, the impedance of NS-0 half-cell significantly changes after the 50th cycle, while the impedance of NS-450 half-cell remains constant. LSV data shows good electrochemical stability of 2D TiO_2 nanosheets, without any side reaction in the investigated voltage range (Figure S5). This indicates that the 2D TiO_2 nanosheets facilitate the formation of a stable solid electrolyte interphase, ensuring smooth Li-ion transport. Additionally, SEM images were analyzed before and after cycling to further understand the electrochemical behavior of the samples (Figure 6). The inhomogeneous surface was observed for bare Cu current collector (Figure 6a-I). As cycling progresses, the surface of the bare copper becomes increasingly non-uniform, indicating inhomogeneous lithium deposition (Figure 6a-II, III), which results in reduced coulombic efficiency for the NS-0 half-cell. On the other hand, the NS-450 half-cell shows relatively smooth and dense lithium deposition even after the 50th and 100th cycles (Figure 6b-II, III), leading to superior electrochemical performance. It is interesting to note that Li was uniformly and densely deposited even at higher current densities of 2 and 3 mA/cm^2 (Figure S6). This verifies that 2D TiO_2 nanosheets are instrumental in regulating Li ion deposition.

Finally, both 2D TiO_2-coated and uncoated current collectors were integrated into a full-cell configuration with LFP as the cathode with loading mass of 5.64 mg/cm^2. Figure 7 presents the charge/discharge profiles of NS-0 and NS-450 at a 1.0 C-rate and 25 °C. The initial discharge capacities were 127 and 131 mAh/g for NS-0 and NS-450, respectively. After 150 cycles, NS-450 exhibits a discharge capacity of 134 mAh/g with high retention. Additionally, we tested an anodeless cell configuration, as shown in Figure S7. The NS-450 anodeless cell demonstrated a significantly improved discharge capacity of 120 mAh/g, compared to 75 mAh/g for the NS-0 anodeless cell during the first discharge. This confirms that the 2D TiO_2-coated nanosheets not only promote uniform lithium deposition but also suppress dendrite growth, resulting in an extended cycling life.

Conclusions

The uniform coating of 2D TiO_2 nanosheets of varying thicknesses onto a copper substrate via electrophoresis has been successfully demonstrated. These modified current collectors were evaluated in a half-cell configuration to assess their

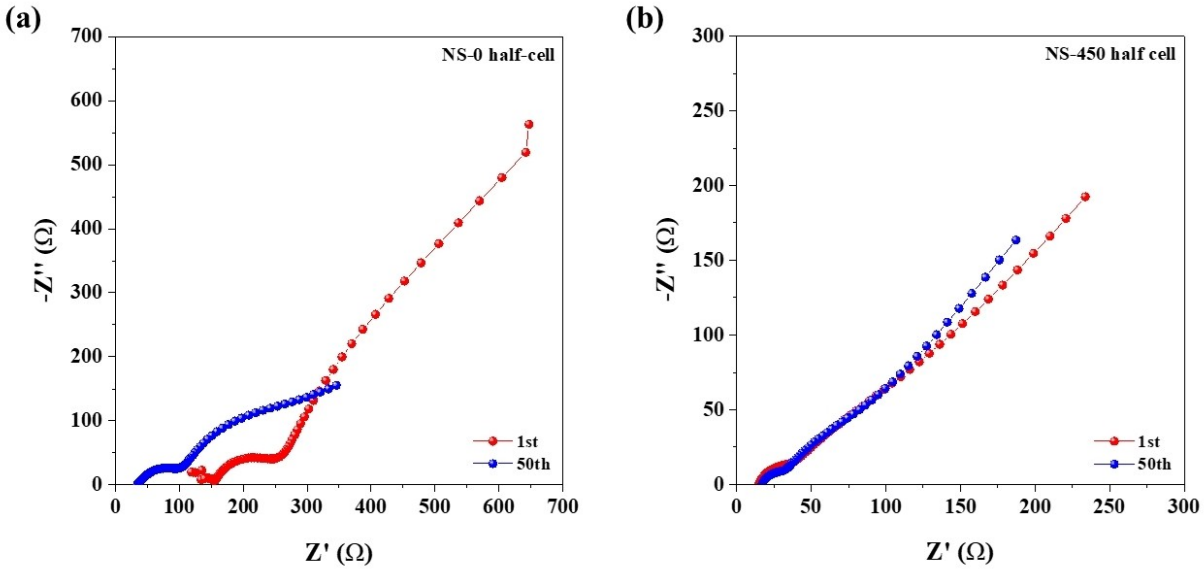

Figure 5. EIS plot for (a) Li|NS-0 and (b) Li|NS-450 after 1st and 50th cycle at current density of 2 mA/cm^2 and areal capacity of 1 mAh/cm^2.

Research Article
doi.org/10.1002/batt.202400741
Chemistry Europe
European Chemical Societies Publishing

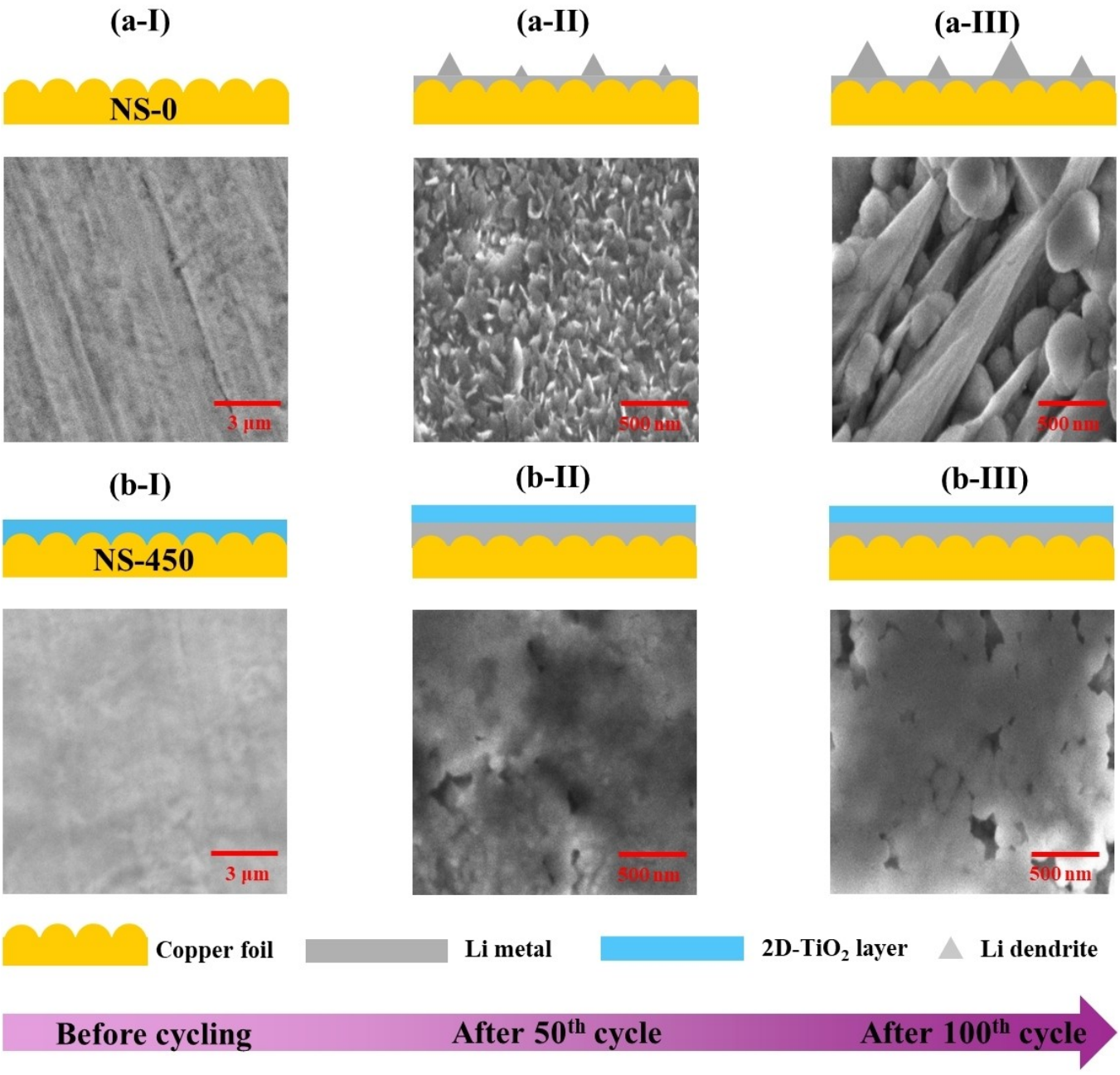

Figure 6. Li growth behavior NS-0 half-cell and NS-450 half cell. Schematic and SEM image of (a-I) NS-0, (b-I) NS-450 surface. Lithium cross-section images (a-II) and (b-II) of NS-0 and NS-450 after 50 cycles at a current density of 1 mA/cm^2 and an area capacity of 1 mAh/cm^2. And lithium cross-section images (a-III) and (b-III) after 100th cycle.

charge-discharge cycling characteristics. The half-cell with the 2D TiO_2 film shows improved cycling performance compared to its uncoated counterpart. Specifically, the cell coated with a 450 nm-thick 2D TiO_2 demonstrates outstanding cycling stability >255 cycles, with an impressive Coulombic efficiency of ~92% at 1 mA/cm^2 and 1 mAh/cm^2. The full cell containing NS-450 samples coupled with LFP cathode showed good capacity retention, associated with reduced surface roughness and low nucleation potential. Hence, the utilization of TiO_2 nanosheets presents a promising strategy for suppressing dendrite formation in lithium metal batteries.

Experimental

The 2D TiO_2 nanosheets were prepared using a previously reported top-down method.[37] The parent phase, $K_{0.8}Ti_{1.73}Li_{0.27}O_4$ (KTLO), was synthesized using the flux method. Raw powders of TiO_2 (99.9%, Grand C&M), K_2CO_3 (99.5%, Samchun Chemicals), Li_2CO_3 (99.0%, Junsei), and MoO_3 (99.5%, Samchun Chemicals) were ball-milled together. Single crystal KTLO was chemically exfoliated to obtain nanosheets. Micrometer-sized 2D TiO_2 nanosheets with a few nanometers thickness were obtained using a combination of acid treatment and organic treatment processes. The acidic treatment KTLO was carried out in 1 M HCl to exchange alkali ions (K^+, Li^+) with hydronium ions, resulting in the formation of hydrated TiO_2

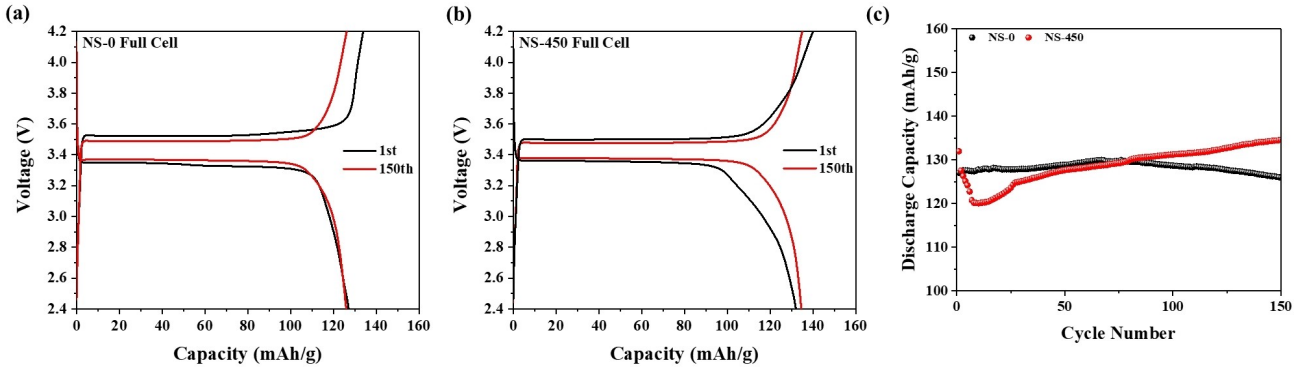

Figure 7. Electrochemical performances of Full cell (a) Li|NS-0|LFP (b) Li|NS-450|LFP (c) Long-term capacity retention of Li|NS-0|LFP and Li|NS-450|LFP at 1.0 C-rate.

($TiO_2 \cdot nH_2O$, HTO). To further increase the interlayer spacing of HTO and facilitate exfoliation, an organic treatment was performed using tetrabutylammonium hydroxide (TBAOH), a large organic molecule that intercalates between the layers. The organic impurities were removed by a dialysis process adopted for 14 days. The morphology of the bulk sample was analyzed by optical microscopy, and the microstructure of the nanosheets was examined by transmission electron microscopy (TEM, JEM-ARM-200F, JEOL), atomic force microscopy (AFM, Dimension 3100, Veeco) and X-ray diffraction (XRD, MiniFlex 600, Rigaku). Microstructural analysis using scanning electron microscopy (SEM, Apreo S HiVac, FEI Company) was also performed.

To investigate the effect of 2D TiO_2 on the electrochemical cycling characteristics of lithium batteries, half cells (2032-coin cells) were fabricated. First, 2D TiO_2 was coated on a copper substrate (current collector) by electrophoresis (a Cu commercial substrate was used; copper substrate (UACJ Foil Corp). The thickness of the substrate was ~18 μm and the area was ~2 cm×5 cm. The substrate was cleaned before use, and the substrate distance of ~1 cm in the solution (2D TiO_2 and water) during electrophoresis was maintained. The nanosheets of different thicknesses were coated by applying voltage in the range of 0–8 V using a d.c. source (Keithley 487). The coated 2D TiO_2 protective layer on the Cu was dried for 24 h at room temperature. The modified Cu current collector was then punched and used (punching diameter ~15 mm) as electrode. 1 M lithium bis(trifluoromethanesulonyl)imide (LiTFSI) in 1,3-dioxolane (DOL)/dimethyl ether (DME) (1:1, v/v, Dongwha Electrolyte) was used as the electrolyte. The commercial Li foil with a thickness of 200 μm was utilized as the counter electrode. Electrochemical characterization was carried out using a battery cycler (WBCS3000Le32, WonAtech). First, a low current was applied from 0.02 to 1 V for 10 cycles to form a stable SEI. The charge and discharge studies were then performed at a current density of 1 mA/cm^2 and an areal capacity of 1 mAh/cm^2 under a cut-off voltage of 1.5 V.

Supporting Information

XRD patterns of 2D TiO_2 nanosheet, The zeta potential of 2D TiO_2, Bending test result, Electrochemical properties of NS-0 and NS-450 half-cell at various current density and areal capacity 1 mAh/cm^2, SEM images of NS-450 after Li deposition at 1 mAh/cm^2, Li growth behavior NS-0 half-cell and NS-450 half cell, anodeless cell test result.

Acknowledgements

This research was supported by the National Research Foundation of Korea (NRF) funded by the Korean government (MSIT) (No. RS-2023-00236572, No. RS-2023-00249335, No. RS-2024-00220).

Conflict of Interests

The authors declare no conflict of interest.

Data Availability Statement

The data that support the findings of this study are available from the corresponding author upon reasonable request.

Keywords: Dendrite growth prevention · TiO_2 Nanosheet · Surface roughness · Cycling · Electrochemical resistance

[1] B. Liu, J. Zhang, W. Xu, *Joule* **2018**, *2*, 833–845.
[2] Y. An, Y. Tian, C. Liu, S. Xiong, J. Feng, Y. Qian, *ACS Nano* **2022**, *16*, 4560–4577.
[3] J. Tarascon, M. Armand, *Nature* **2001**, *414*, 359–367.
[4] D. Lin, Y. Liu, Y. Cui, *Nat. Nanotechnol.* **2017**, *12*, 194–206.
[5] W. Xu, J. Wang, F. Ding, X. Chen, E. Nasybulin, Y. Zhang, J. Zhang, *Energy Environ. Sci.* **2014**, *7*, 513–537.
[6] L. Ye, M. Liao, X. Cheng, X. Zhou, Y. Zhao, Y. Yang, C. Tang, H. Sun, Y. Gao, B. Wang, H. Peng, *Angew. Chem. Int. Ed.* **2021**, *60*, 17419.
[7] X. Cheng, R. Zhang, C. Zhao, Q. Zhang, *Chem. Rev.* **2017**, *117*, 10403–10473.
[8] Q. Yun, Y. He, W. Lv, Y. Zhao, B. Li, F. Kang, Q. Yang, *Adv. Mater.* **2016**, *28*, 6932–6939.
[9] J. H. Suh, D. K. Kim, M. S. Park, *Ceramist.* **2023**, *26*, 265–279.
[10] S. Wei, S. Choudhury, Z. Tu, K. Zhang, L. A. Archer, *Acc. Chem. Res.* **2018**, *51*, 80–88.
[11] Y. Guo, H. Li, T. Zhai, *Adv. Mater.* **2017**, *29*, 1700007.
[12] M. Nasir, J. Seo, J. S. Park, H. J. Park, *J. Eur. Ceram. Soc.* **2024**, *44*, 4606–4611.
[13] M. Nasir, J. Y. Park, P. Heo, K. H. Choi, H. J. Park, *Adv. Funct. Mater.* **2023**, *33*, 2303397.
[14] S. B. Park, *Ceramist.* **2022**, *26*, 104–121.
[15] M. D. Tikekar, S. Choudhury, Z. Tu, L. A. Archer, *Nat. Energy* **2016**, *1*, 1–7.
[16] L. Chen, A. Lv, F. Guo, M. Wang, S. Jiao, *ACS Sustainable Chem. Eng.* **2019**, *8*, 706–713.

[17] N. Li, Y. Yin, C. Yang, Y. Guo, *Adv. Mater.* **2016**, *28*, 1853–1858.
[18] H. Lee, X. Ren, C. Niu, L. Yu, M. H. Engelhard, I. Cho, M. Ryou, H. S. Jin, H. Kim, J. Liu, *Adv. Funct. Mater.* **2017**, *27*, 1704391.
[19] S. Liu, S. X. Xia, Y. Zhong, S. Deng, Z. Yao, L. Zhang, X. Cheng, X. Wang, Q. Zhang, J. Tu, *Adv. Energy Mater.* **2018**, *8*, 1702322.
[20] Z. Wang, Z. S. Lu, K. Lu, Y. Li, R. Wang, Y. Cheng, W. Qin, X. J. Wu, *Power Sources* **2019**, *428*, 1–7.
[21] K. Yan, B. Sun, P. Munroe, G. Wang, *Energy Storage Mater.* **2018**, *11*, 127–133.
[22] Z. Hou, Y. Yu, W. Wang, X. Zhao, Q. Di, Q. Chen, W. Chen, Y. Liu, Z. Quan, *ACS Appl. Mater. Interfaces* **2019**, *11*, 8148–8154.
[23] C. Zhang, W. Lv, G. Zhou, Z. Huang, Y. Zhang, R. Lyu, H. Wu, Q. Yun, F. Kang, Q. Yang, *Adv. Energy Mater.* **2018**, *8*, 1703404.
[24] C. Sun, Y. Li, J. Jin, J. Yang, Z. Wen, *J. Mater. Chem. A. Mater.* **2019**, *7*, 7752–7759.
[25] F. Shen, F. Zhang, Y. Zheng, Z. Fan, Z. Li, Z. Sun, Y. Xuan, B. Zhao, Z. Lin, X. Gui, *Energy Storage Mater.* **2018**, *13*, 323–328.
[26] H. Fan, Q. Dong, C. Gao, B. Hong, Y. Lai, *Mater. Lett.* **2019**, *234*, 69–73.
[27] Y. Xu, A. S. Menon, P. P. R. Harks, D. C. Hermes, L. A. Haverkate, S. Unnikrishnan, F. M. Mulder, *Energy Storage Mater.* **2018**, *12*, 69–78.
[28] Z. Xu, L. Xu, Z. Xu, Z. Deng, X. N. Wang, *Adv. Funct. Mater.* **2021**, *31*, 2102354.
[29] Z. Lu, Z. Tai, Z. Yu, A. P. LaGrow, O. Bondarchuk, J. P. Sousa, L. Meng, Z. Peng, L. Liu, *Mater. Today Energy* **2021**, *22*, 100871.
[30] R. Li, J. Wang, L. Lin, H. Wang, C. Wang, C. Zhang, C. Song, F. Tian, J. Yang, Y. Qian, *Mater. Today Energy* **2020**, *15*, 100367.
[31] K. Pu, X. Zhang, X. Qu, J. Hu, H. Li, M. Gao, H. Pan, Y. Liu, *Rare Met.* **2020**, *39*, 616–635.
[32] Z. Ouyang, S. Wang, Y. Wang, S. Muqaddas, S. Geng, Z. Yao, X. Zhang, B. Yuan, X. Zhao, Q. Xu, *Adv. Mater.* **2024**, *36*, 2407648.
[33] Y. Wang, Z. Qu, S. Geng, M. Liao, L. Ye, Z. Shadike, X. Zhao, S. Wang, Q. Xu, B. Yuan, *Angew. Chem.* **2023**, *135*, e202304978.
[34] P. K. Sharma, V. Sharma, R. S. Rajaura, S. Srivastava, S. S. Sharma, M. Singh, Y. K. Vijay, *AIP Conf. Proc.* **2016**, *1728*, 020531.
[35] A. Mohammadi, L. Monconduit, L. Stievano, R. Younesi, *J. Electrochem. Soc.* **2022**, *169*, 070509.
[36] C. Huang, B. Thirumalraj, H. Tao, K. N. Shitaw, H. Sutiono, T. T. Hagos, T. T. Beyene, L. Kuo, C. Wang, S. Wu, *Nat. Commun.* **2021**, *12*, 1452.
[37] S. E. Lee, S. Y. Jung, J. Seo, J. H. Joo, J. Lee, Y. Kim, K. H. Lee, Y. I. Kim, H. J. Park, *Adv. Mater. Interfaces.* **2021**, *8*, 21011.

Manuscript received: November 20, 2024
Revised manuscript received: December 17, 2024
Accepted manuscript online: December 23, 2024
Version of record online: January 10, 2025